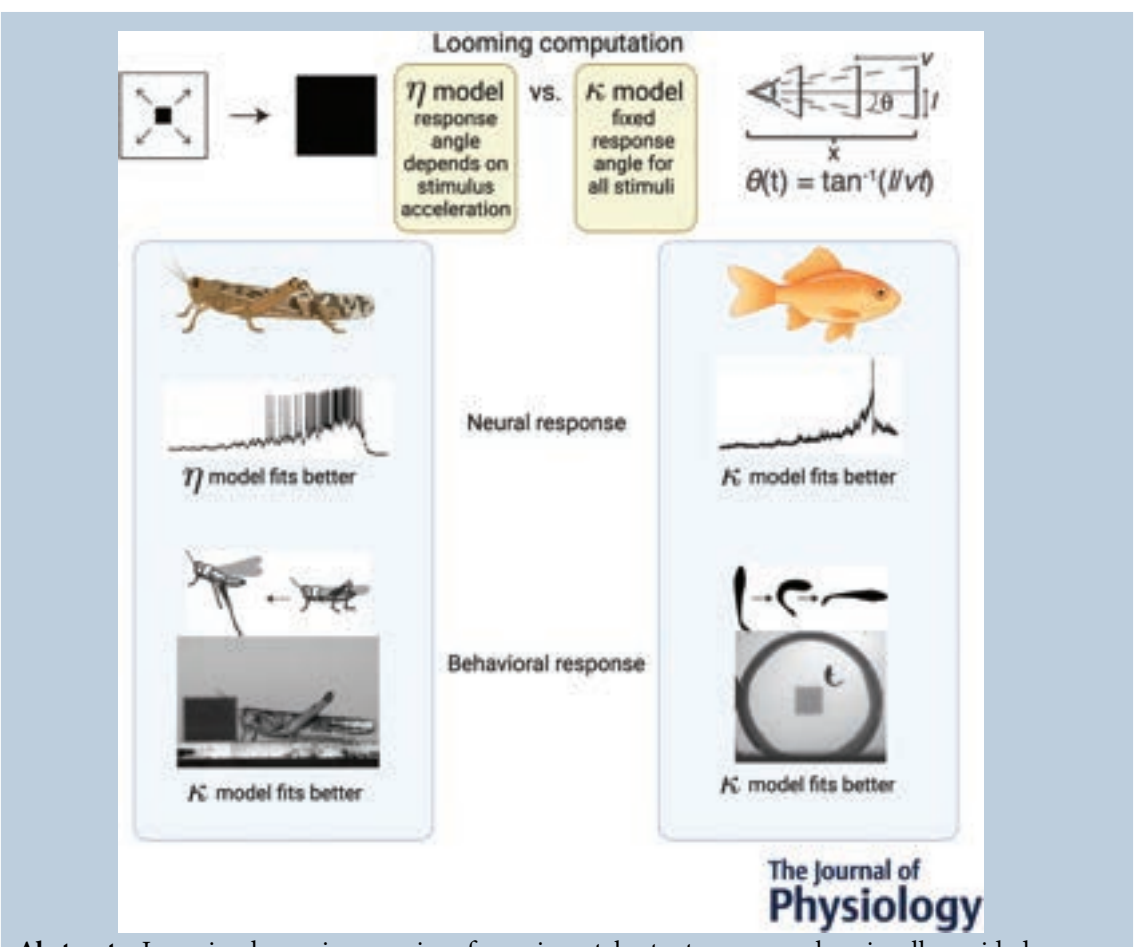
Check for updates

Convergent escape behaviour from distinct visual processing of impending collision in fish and grasshoppers

Richard B. Dewell¹, Terri Carroll-Mikhail², Margaret R. Eisenbrandt¹, Alexander F. Mendoza¹, Bidisha Halder¹, Thomas Preuss² and Fabrizio Gabbiani¹

Handling Editors: David Wyllie & Vatsala Thirumalai

The peer review history is available in the Supporting Information section of this article (https://doi.org/10.1113/JP284022#support-information-section).



Abstract In animal species ranging from invertebrate to mammals, visually guided escape behaviours have been studied using looming stimuli, the two-dimensional expanding projection on a screen of an object approaching on a collision course at constant speed. The peak firing rate

¹Department of Neuroscience, Baylor College of Medicine, Houston, TX, USA

²Hunter College and the Graduate Center, The City University of New York, New York, USA

R. B. Dewell and T. Carroll-Mikhail are co-first authors.

T. Preuss and F. Gabbiani contributed equally to this work.

This article was first published as a preprint. Dewell RB, Carroll-Mikhail T, Eisenbrandt MR, Preuss T, Gabbiani F. 2022. Convergent escape behavior from distinct visual processing of impending collision in fish and grasshoppers. bioRxiv. https://doi.org/10.1101/2022.10.26.513903

or membrane potential of neurons responding to looming stimuli often tracks a fixed threshold angular size of the approaching stimulus that contributes to the triggering of escape behaviours. To study whether this result holds more generally, we designed stimuli that simulate acceleration or deceleration over the course of object approach on a collision course. Under these conditions, we found that the angular threshold conveyed by collision detecting neurons in grasshoppers was sensitive to acceleration whereas the triggering of escape behaviours was less so. In contrast, neurons in goldfish identified through the characteristic features of the escape behaviours they trigger, showed little sensitivity to acceleration. This closely mirrored a broader lack of sensitivity to acceleration of the goldfish escape behaviour. Thus, although the sensory coding of simulated colliding stimuli with non-zero acceleration probably differs in grasshoppers and goldfish, the triggering of escape behaviours converges towards similar characteristics. Approaching stimuli with non-zero acceleration may help refine our understanding of neural computations underlying escape behaviours in a broad range of animal species.

(Received 27 October 2022; accepted after revision 10 August 2023; first published online 6 September 2023)

Correspondence author F. Gabbiani: Department of Neuroscience, Baylor College of Medicine, Houston, TX 77030, USA. Email: gabbiani@bcm.edu

Abstract figure legend Responses to looming stimuli were measured in grasshoppers and goldfish to test predictions made by competing models of looming detection. Both models predict similar timing of response for stimuli simulating approach with constant velocity (ν), but differ in predictions of responses to stimuli with accelerating or decelerating approach. The κ model predicts responses to all stimuli after a constant angular threshold size (θ), while the η model predicts a shift in response angle dependent on stimulus acceleration. For grasshoppers, neural responses were best described by the η model, but their behavioural timing was better described by the κ model. The fish showed no shift in response timing with acceleration as predicted by the κ model.

Key points

- A companion manuscript showed that two mathematical models of collision-detecting neurons in grasshoppers and goldfish make distinct predictions for the timing of their responses to simulated objects approaching on a collision course with non-zero acceleration.
- Testing these experimental predictions showed that grasshopper neurons are sensitive to
 acceleration while goldfish neurons are not, in agreement with the distinct models proposed previously in these species using constant velocity approaches.
- Grasshopper and goldfish escape behaviours occurred after the stimulus reached a fixed angular size insensitive to acceleration, suggesting further downstream processing in grasshopper motor circuits to match what was observed in goldfish.
- Thus, in spite of different sensory processing in the two species, escape behaviours converge towards similar solutions.
- The use of object acceleration during approach on a collision course may help better understand the neural computations implemented for collision avoidance in a broad range of species.

Richard Dewell is a neuroethologist that has been studying mechanisms underlying neural processing since his undergraduate studies in cognitive neuroscience at Washington University in St. Louis. He examined the role of synaptic plasticity in motor control of crabs during his Ph.D. at Louisiana State University and has since been studying looming detection and escape behavior in insects at Baylor College of Medicine, first as a postdoctoral fellow and now as a research assistant professor.



14697793, 2023, 19, Downloaded from https://physoc.onlinelibrary.wiley.com/doi/10.1113/JP284022 by University Of Texas - Ham/Tmc, Wiley Online Library on [24.05/2024]. See the Terms and Conditions

and-conditions) on Wiley Online Library for rules of use; OA articles are governed by the applicable Creative Commons License

14697793, 2023, 19, Downloaded from https://physoc.onlinelibrary.wiley.com/doi/10.1113/JP284022 by University Of Texas - Ham/Tmc, Wiley Online Library on [24.05/2024]. See the Terms and Conditions

and-conditions) on Wiley Online Library for rules of use; OA articles are governed by the applicable Creative Commons I

Introduction

For visual detection of impending threats, diverse animal groups, including mammals, fish, insects, crustaceans and birds possess neurons that specifically respond to visual looming stimuli, i.e. objects approaching on a collision course with constant velocity (Bennett et al., 2019; Bhattacharyya et al., 2017; de Vries & Clandinin, 2012; Dunn et al., 2016; Fotowat et al., 2009; Liu et al., 2011; Nakagawa & Hongjian, 2010; Oliva & Tomsic, 2014; Preuss et al., 2006; Sun & Frost, 1998; Temizer et al., 2015; Wu et al., 2005). These studies showed that the evoked escape behaviour to visual looms differs between species, while response timing is often, but not always, comparable (Branco & Redgrave, 2020; Hemmi & Tomsic, 2012). This raises the question of how different the neural computations that determine the timing of the behaviour are.

Fish and grasshoppers react to visual looms, either with a powerful startle escape - triggered by a body bend (C-start) - or with a prepared jump, propelling them away from the perceived threat (Fig. 1A and B; for C-starts in fish, see Domenici & Hale, 2019; Preuss et al., 2006; for jumps in grasshoppers, see Fotowat & Gabbiani, 2007; Fotowat et al., 2011). In fish, startle escapes to an overhead loom are typically initiated by a single action potential in one of the paired Mauthner cells (M-cells), which determines the timing and direction of the response (Fig. 1C). Loom stimuli presented from various directions, including from the front, or side also trigger escape behaviours in loosely restrained and freely moving zebrafish (Bhattacharyya et al., 2017; Temizer et al., 2015). Recordings from the M-cell ventral (visual) dendrite and chronic recordings from M-cell axons in freely behaving fish showed that peak M-cell membrane depolarization and action potentials in response to looms are tightly correlated and consistently occur just before collision time (Fig. 1Cb and c; Preuss et al., 2006; Weiss et al., 2006). In other words, the timing of C-starts measured behaviourally reliably indicates the preceding peak time of M-cell membrane depolarization.

In grasshoppers, escape behaviour to simulated objects approaching from the side (Fig. 1Da) is triggered by the activation of an identified neuron called the descending contralateral movement detector (DCMD) which faithfully relays the firing pattern of the lobula giant movement detector (LGMD) neuron to motor circuits (O'Shea & Williams, 1974; O'Shea et al., 1974). In contrast to fish, the LGMD/DCMD neurons must generate sustained firing to trigger successful escape (Fig. 1Db; Fotowat et al., 2011). This sustained firing (~200 ms) probably contributes to escape jump preparation (Fotowat & Gabbiani, 2011). Yet, the firing rate of the DCMD neuron has a similar shape as the Mauthner cell's membrane potential, peaking and decaying before

projected collision time (Fig. 1Cb and Db; Gabbiani et al., 1999).

Two distinct models have been proposed to describe the responses of goldfish and grasshoppers to simulated objects approaching at a constant speed towards the animal (Gabbiani et al., 1999; Hatsopoulos et al., 1995; Preuss et al., 2006). Here, we studied the neural responses predicted by these models to simulated accelerating approaching objects that have not yet been employed either in behavioural, or in electrophysiological experiments (see Gabbiani et al., 2023). The same stimuli were used to compare and contrast the behavioural responses of fish and grasshoppers. We thus start by describing and comparing these novel accelerating stimuli to conventional constant speed looming stimuli. While

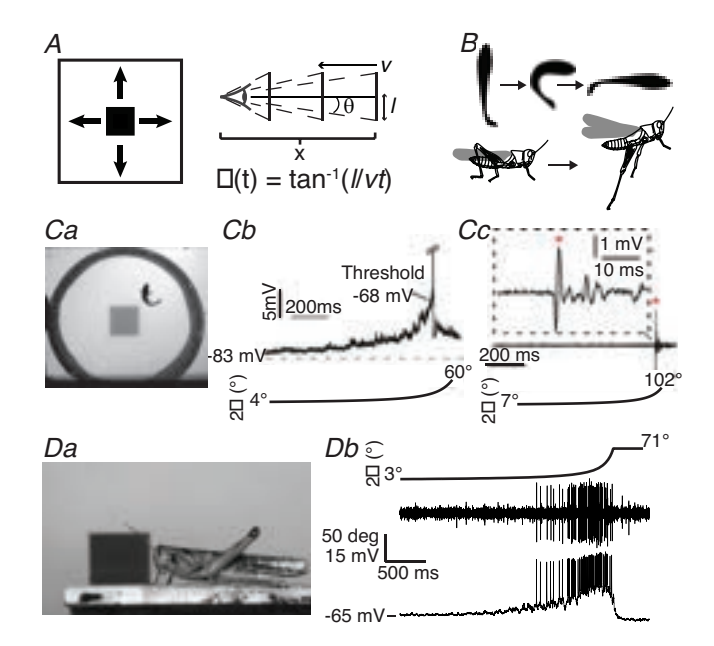


Figure 1. Fish and grasshoppers' responses to looming stimuli A, left, illustration of a black looming stimulus, simulating a solid square with half-size / approaching with constant velocity v. Right, the ratio $\gamma = I/v$ defines the angular half-size of the object $\theta(t)$ at time t relative to collision, B, schematic illustrations of fish (top) and grasshopper (below) escape responses to looming stimuli. Ca, ventral view of goldfish startle behaviour (C-start) in response to a looming stimulus presented from above. Cb, intracellular recorded M-cell membrane potential in response to a looming stimulus (stimulus angular size shown below). Cc, extracellular recording of M-axon field potentials in a freely behaving goldfish shows a single M-cell spike (*, magnified in dashed rectangular inset) preceding a loom-evoked C-start (not shown). Note that in both b and c the Mauthner cell spike occurs shortly before the end of loom expansion (modified from Preuss et al., 2006, and Weiss et al., 2006). Da, image of a grasshopper being presented a looming stimulus from the side, taken before the animal jumped and flew away. Db, example simultaneous extracellular recording of DCMD spiking (middle) and intracellular LGMD membrane potential (bottom) during the final 3 s of a looming stimulus presentation (top). The LGMD responds with high frequency firing that peaks shortly before the end of expansion.

the grasshopper and goldfish models make identical predictions for looming stimuli, they make distinct predictions for responses to accelerating stimuli, allowing us to tease them apart and to better understand the differences in the neural computations implemented in these two model systems.

Methods

Ethical approval

The fish behavioural experiments for the current study involved individual free-swimming animals responding to visual stimuli evoking a startle escape response. Fish were not exposed to manipulations that cause pain. The experiments were performed in accordance with an approval of the Institutional Animal Care and Use Committee (IACUC) of Hunter College, New York (Code: TP-inhibition 12/20). The electrophysiology data shown here are from previous published work and were performed in accordance with an approval by the IACUC of Albert Einstein College of Medicine, New York. IACUC Committees follow federal guidelines from the Office of Laboratory Animal Welfare (https://olaw.nih.gov/resources/tutorial/iacuc.htm).

Animals

Grasshopper experiments were conducted with adult *Schistocerca americana*, 8–12 weeks of age. Animals were reared in a crowded laboratory colony under 12-h light/dark conditions. Preference was given to large, active females \sim 3 weeks after their final moult. No differences were observed between sexes, but the larger size of females make them easier to work with.

Fish experiments used nineteen naive goldfish (*Carassius auratus*) of mixed sex, between 8.0 and 8.5 cm in body length, purchased from Ozark Fisheries, Stoutland, MI, USA. Fish were maintained according to the guidelines and regulations of the Hunter College Institutional Animal Care and Use Committee (IACUC). The animals were kept in three holding tanks (95 l; $30 \times 30 \times 60$ cm) connected to a recirculating filter system (Fluval 207) that used conditioned water (pH: 7.2–7.6, conductivity: 200– $300~\mu$ S; temperature: $19~\pm~1~$ °C), under 12-h light/dark conditions. Fish were fed floating pellets or flakes (Tetra) *ad libitum* for 30 min five times a week. Remaining food was removed after 30 min. Behavioural experiments were performed after acclimation for at least 2 weeks.

Visual stimuli

We used three broad types of stimuli for behavioural and electrophysiological experiments in fish and

grasshoppers: (i) looming stimuli with constant approach velocity; (ii) stimuli with constant, non-zero acceleration designed to 'collide' with the experimental subject at the same time as looming stimuli; and (iii) stimuli with constant angular speed of expansion simulating an approach with pronounced, non-linear deceleration. In all cases, the stimuli simulated, on a two-dimensional screen, an object approaching on a collision course towards the experimental subject. Yet, the three types of stimuli differ substantially in their approach trajectories, as detailed below. The first two types of stimuli were used to compare the timing of peak neuronal responses and of behaviour to the predictions of the η and κ models previously used for grasshoppers and goldfish, respectively (see Results). The third stimulus type was required to further distinguish the two models for grasshopper electrophysiological and behavioural data. See Gabbiani et al., 2023, for a detailed description of the stimuli and predicted responses.

Classically, looming stimuli (looms) have been defined as the two-dimensional simulation of objects approaching at a constant speed on a collision course with the animal (Schiff et al., 1962). For a solid square object of half-size l, starting at an initial distance x_i from the eye, the distance from the eye as a function of time $s \ge 0$ measured from movement onset is described by

$$x(s) = vs + x_i$$

14697793, 2023, 19, Downloaded from https://physoc.onlinelthray.wiley.com/doi/10.113/IP284022 by University Of Texas - Ham/Imc, Wiley Online Library on [2405/2024]. See the Terms and Conditions (https://onlinelthrary.wieley.com/terms-and-conditions) on Wiley Online Library for rules of use; OA atticles are governed by the applicable Creative Commons License

where v < 0 is the approach speed. It will be useful to define a (dimensionless) normalized distance y(s) = x(s)/l in terms of the stimulus half-size so that

$$y(s) = s/\gamma + y_i, y_i = x_i/l.$$

The constant $\gamma = l/v < 0$ (in units of time) fully characterizes the approach trajectory as perceived at the animal's eye (Gabbiani et al., 1999). In earlier work we have used the absolute value of γ , $l/|\nu|$ which provides an equivalent description, but the use of γ is more convenient in mathematical formulas. The time of collision $s_c = -\gamma y_i > 0$ is obtained by solving the equation $\gamma(s) = 0$. If time is referenced relative to collision, $t = s - s_c$, then $\gamma(t) = t/\gamma$ and the half-angle subtended by the object at the retina is obtained by trigonometry as $\tan^{-1}(l/\nu t)$ or

$$\theta(t) = \tan^{-1}(1/y(t)). \tag{1}$$

The five stimuli used are illustrated in Fig. 2A and B (green lines, $\gamma = -20, -30, -50, -70,$ and -80 ms).

In our experiments, looming stimuli had an initial subtended half-angle of 0.75° (full angle: 1.5°) and expanded until filling the vertical axis of the screen. The maximum full angle (2θ) values reached by the stimuli were either 136° or 80° for the freely behaving or restrained grasshoppers, respectively, and 102° for the fish.

14697793, 2023, 19, Downloaded from https://physoc.onlinelibrary.wiley.com/doi/10.1113/JP284022 by University Of Texas - Ham/Tmc, Wiley Online Library on [24.05.2024]. See the Terms and Conditions (https://onlinelibrary.wiley.

and-conditions) on Wiley Online Library for rules of use; OA articles are governed by the applicable Creative Commons I

The normalized distance of stimuli with non-zero constant acceleration (NZAs) is given by

$$y(s) = (\rho/2) s^2 + s/\gamma_1 + \gamma_1$$

where $\rho = a/l$ is the normalized acceleration in units of $1/\text{time}^2$ and $1/\gamma_i$ is the initial normalized speed (in units of 1/time). In our experiments, γ_i was always equal to -50 ms. Note that since y(s) > 0 decreases towards collision, $\rho < 0$ represents an accelerating stimulus (since the normalized distance decreases faster than for $\rho = 0$) and $\rho > 0$ a decelerating one (since the decrease in normalized distance will be slower than for $\rho = 0$).

Let us now consider a fixed looming stimulus with projected collision time $s_c = -\gamma_c y_i$. The above equation determines the normalized acceleration ρ required for a stimulus with initial normalized speed $1/\gamma_i$ to achieve the same projected collision time (as

a function of y_i , γ_i and γ_c ; see eqn (13) of Gabbiani et al., 2023). In our experiments, we used two γ_c values to generate accelerating stimuli, $\gamma_c = -20$ ms so that $\rho = -39.3 \text{ s}^{-2}$ and $\gamma_c = -30$ ms so that $\rho = -11.6 \text{ s}^{-2}$. The two decelerating stimuli had $\gamma_c = -70$ ms so that $\rho = 2.14 \text{ s}^{-2}$ and $\gamma_c = -80$ ms so that $\rho = 2.45 \text{ s}^{-2}$. These non-zero acceleration stimuli (NZAs) are illustrated in Fig. 2A and B (dashed lines).

Constant angular velocity stimuli (CAVs) are defined by the equation

$$\theta(s) = \theta_i + \psi s, \quad \psi = (\theta_c - \theta_i)/s_c,$$

where θ_i is the initial angular size, $\theta_c = \pi/2$ is the angular size at projected collision time (in radian), and ψ is the angular velocity in radian/time. If time is referenced relative to collision, this equation becomes

$$\theta(t) = \psi t + \theta_c$$

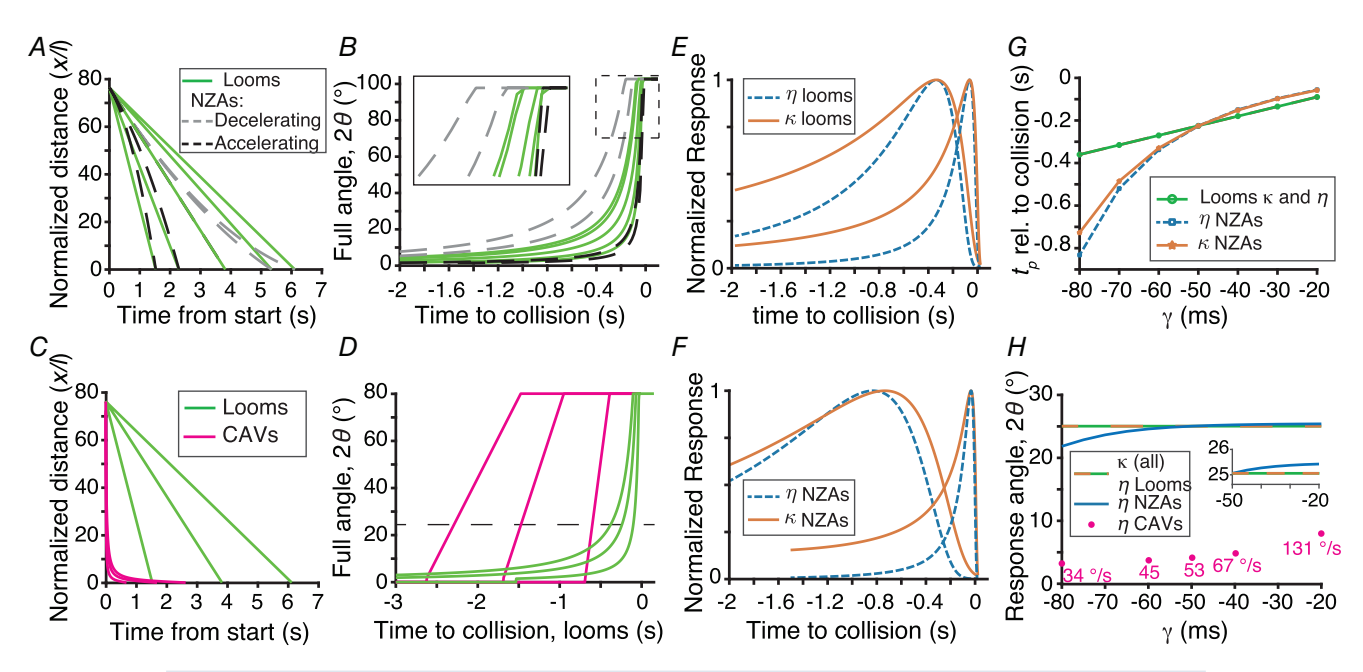


Figure 2. Visual stimuli simulating approaching objects with various velocity profiles and predicted model responses

A, looming stimuli (looms, green) simulate objects approaching at constant velocity (i.e. a linear decrease in normalized distance); non-zero acceleration stimuli (NZAs) either accelerate (black) or decelerate (grey). B, both looms and NZAs have steeply increasing angular sizes around the projected time of collision. The inset magnifies angular trajectories close to collision time shown in the dashed box in the main panel. C, compared to looms, constant angular velocity stimuli (CAVs; magenta lines) simulate faster initial approaches followed by steep deceleration. D, the angular size of CAVs increases linearly and their angular velocity (slope) was selected to match that of looms when 2θ equalled 25° (dashed line). E, normalized time course of η and κ equations for looms with γ of -80 and -20 ms. For η , the plotted parameters were $\alpha=9$ and $\delta=25$ ms; for κ , the parameters were $\beta = 4.573$ and $\delta = 25$ ms. F, normalized time course of η and κ equations for NZAs with γ of -80 and -20 ms. G, the η and κ models predict identical peak response times to looms that are linearly dependent on γ (green), but model-dependent response timings for NZAs (blue and ochre, respectively). H, both the η and κ models predict a fixed peak response angle for looms. The κ model predicts the same peak response angle for NZAs and CAVs (dashed green-ochre line). The η model predicts slight changes for NZAs (blue line) and peak responses at smaller angles for CAVs (magenta dots, with the indicated constant angular velocity). CAVs are not parametrized by ν . hence for the η model, the predicted peak response full angles are plotted aligned to those looming stimulus γ values having matched angular velocity at their respective peak time (see Methods). The inset magnifies the plot for $\gamma > -50$ ms around the models' peak response angle (25°).

and the normalized distance is obtained from eqn (1), $y(t) = 1/\tan\theta(t)$. From the three examples illustrated in Fig. 2C and D (pink lines), it can be seen that such stimuli represent a case of extreme deceleration compared to those considered above. Their normalized speed is largest at the beginning of approach and asymptotes at a value of $-\psi$ at collision time (sec. 6 of Gabbiani et al., 2023).

In grasshopper experiments, the angular velocities used for CAVs were selected to match the angular velocities of looming stimuli near the typical time of the grasshoppers' peak neural response corresponding to a full threshold angle of 25°. For looms with γ of -20, -40, -50, -60 and -80 ms this corresponds to ψ of 131, 67, 53, 45, and 34°/s respectively (Fig. 2*D*, dashed line).

Although the term 'looming stimuli' has been used loosely recently, including for simulated constant angular velocity approaching stimuli, we will reserve our use of the terms 'looming stimuli' and 'looms' to the classical definition (constant approach speed). We will use the abbreviation NZAs for non-zero acceleration stimuli and CAVs for constant angular velocity stimuli.

Grasshopper behavioural experiments

Grasshopper behavioural experiments were conducted as described previously (Dewell & Gabbiani, 2018; Fotowat & Gabbiani, 2007; Fig. 1B and D). Briefly, animals were placed on a short, 2 cm wide platform and walked along it parallel to the monitor. When the animal reached the end of the platform, placing their right eye 6 cm in front of the centre of the screen, a visual stimulus was started manually. The stimuli were generated at 200 Hz with custom C code using the Scitech graphics library on a QNX4 personal computer (PC). A cathode ray tube (CRT) monitor was used to present the stimuli. The luminance of the background was equal to 77 cd/m², while dark simulated approaching objects had a luminance of 2 cd/m². Behavioural responses were recorded with each video frame synched to the stimulus frames. The stimuli were presented in random order, and at least 10 min elapsed between trials of the same animal. In all, there were 1144 trials using 36 animals and 9 stimuli (5 looms and 4 non-zero acceleration stimuli; see above for detailed description of the stimuli). For some of these animals there were not enough trials for meaningful within-animal statistics. Sufficient data were available from 19 animals (972 trials) for detailed within- and across-animal comparisons and these were used for subsequent analysis. For the experiments testing constant acceleration stimuli, 353 trials were recorded from 6 animals, with 10 trials excluded from analysis (see next paragraph).

Grasshopper behavioural data analysis

Jump probability was calculated based on the median unbiased estimator of a binomial response model. The jump timing (and corresponding subtended stimulus angle) were calculated based on the first video frame showing leg extension. Each video was examined to ensure the animal was properly positioned to see the stimulus, and trials in which the animal jumped or turned away before stimulus presentation were excluded. There weren't enough trials to determine α and δ parameters of the η model for individual animals, so the δ used in threshold angle calculations was the same for all animals (see Results). The values were calculated by a weighted least squared-error linear fit of the behavioural jump time, $t_{\rm b}$, to looms as a function of the stimulus parameter, γ (Fotowat & Gabbiani, 2007; Gabbiani et al., 1999; see also Grasshopper electrophysiological data analysis below).

Grasshopper electrophysiological experiments

For grasshopper electrophysiology, animals were placed ventral side up in a plastic holder with the left eye 18 cm from the stimulus monitor. The neck membrane was removed to expose the ventral nerve cord. Wires 50 μ m in diameter were placed around the right nerve cord such that de-insulated wire was in contact with its dorso-medial surface allowing recording of action potentials from the descending contralateral movement detector (DCMD) axon coursing from the head to the thorax (Fig. 1*D*).

14697793, 2023, 19, Downloaded from https://physox.onlinelibrary.wiley.com/doi/10.1113/IP284022 by University Of Texas - Ham/Imc, Wiley Online Library on [24.05/2024]. See the Terms and Conditions (https://onlinelibrary.wiley.com/terms-and-conditions) on Wiley Online Library for rules of use; OA articles are governed by the applicable Creative Commons License

The same stimuli used in behavioural experiments were shown in randomized blocks with 2 min between stimuli. To prevent habituation, animals were exposed to regular visual, auditory and mechano-sensory stimulation between trials consisting of flashing room lights, shaking of keys, and stroking the abdomen as has been used in previous experiments. Responses to non-zero acceleration and looming stimuli were recorded from 11 animals. Responses to constant angular velocity and looming stimuli were recorded from 7 animals. Previous experiments recording DCMD responses to looming stimuli have found the firing pattern remains consistent independent of animal orientation, distance to the screen, or level of restraint (Dewell & Gabbiani, 2018; Fotowat et al., 2011; Gabbiani et al., 2001). Thus, it is unlikely that the different positioning of the animals in behaviour and electrophysiology experiments influence the results.

Grasshopper electrophysiological data analysis

Extracellular recordings of DCMD activity were analysed as previously described (Dewell & Gabbiani, 2018; Gabbiani et al., 1999). Briefly, DCMD action potentials were determined by amplitude thresholding, and the instantaneous firing rate (IFR) was calculated by

14697793, 2023, 19, Downloaded from https://physoc.onlinelibrary.wiley.com/doi/10.1113/JP284022 by University Of Texas - Ham/Tmc, Wiley Online Library on [24.05.2024]. See the Terms and Conditions (https://onlinelibrary.wiley

and-conditions) on Wiley Online Library for rules of use; OA articles are governed by the applicable Creative Commons License

convolving the spike raster of each trial with a Gaussian filter having a standard deviation of 20 ms. The time of the peak response (t_p) was measured as the time of the peak IFR relative to the projected time of stimulus collision. Normalized IFRs (Fig. 8H) were calculated by taking the mean IFR across animals in response to each stimulus and then dividing that by its peak value. This allowed to easily visualize the percentage of firing rate decay from the peak at the times of jump.

The α and δ parameters of the η model fits for looming stimuli were determined by a weighted least squared-error linear fit of the peak response time, $t_{\rm p}$, as a function of the stimulus parameter, γ . The parameter δ is the γ -intercept of the fit, α is twice the slope (Gabbiani et al., 2023). The threshold angle was determined as the stimulus angular size at $t_{\rm p}-\delta$ (Gabbiani et al., 1999). Fits of the η model for combined responses of looms and non-zero acceleration stimuli were determined using the Matlab least squared error minimization function 'lsqcurvefit'.

Fish experimental set-up

Fish experiments were conducted in a tank measuring 77 cm in diameter and 30.5 cm in height that contained a round mesh arena insert of 39 cm in diameter and 27.6 cm in height. The tank was filled with conditioned water that matched that of the holding tanks. Fish were introduced to the tank and were free to swim around within the arena; however, the water height (7.5 cm) confined their movement to a two-dimensional plane. A translucent white plastic lid on top of the tank served as projection screen for visual stimuli (screen-water surface distance 22.5 cm). The set-up was situated on an anti-vibration table behind a curtain to avoid unintended mechano-sensory and visual stimuli.

Visual stimuli were projected on the screen with a digital light processing (DLP) projector $(1024 \times 768 \text{ pixels}, 60 \text{ Hz}; \text{U4-131 Plus}, \text{Vision Corp.},$ Tokyo, Japan). The location onset of the visual loom was varied between four positions. They were generated on a PC running the Windows operating system using Matlab and the Psychtoolbox (PTB-3). Overhead projection simulated predator approach relevant to Carassius auratus (Vijayan et al., 2018). At the screen, the luminance of the background was 18 cd/m² and that of the visual stimulus simulating dark approaching objects was 2 cd/m². To avoid habituation, inter-stimulus intervals were randomized between 2 and 7 min. In addition, audio sound pips were delivered at random intervals for dishabituation (200 Hz; 5 ms; 158 dB rel. to 1 μ Pa in water). These stimuli were produced by a stimulator (Master-8, A.M.P.I., Jerusalem, Israel), amplified (Servo 120, Samson Technologies, Hickville, NY, USA), and delivered via either one of two underwater loudspeakers (Model UW30, Electro-Voice, Burnsville, MN, USA). To analyse the latency and kinematics of evoked startle escape behaviour, a ventral view of the fish was recorded at 250 frame/s with a high-speed camera (AOS Technologies AG, Daettwil, Switzerland) and analysed with imaging software (Imaging Studio, AOS Technologies AG, and ImageJ, NIH, Bethesda, MD, USA).

Fish behavioural experiment design

Individual fish were transferred from the holding tank to the experimental tank and acclimated for 15 min. In a first set of experiments, each animal (N = 9) was exposed in 27 trials (\pm 2) to nine different visual stimuli (\sim 3 trials per stimulus per subject). Stimuli were identical to those presented to grasshoppers, and likewise were presented in blocks with each stimulus shown once per block in random order. Stimulus angles were calculated based on the distance from the screen to the water surface. After an initial analysis of the evoked behaviour, a second experiment (N = 10 animals) focused on three looming stimuli with l/v = -20, -50 and -80 ms, and the corresponding accelerating and decelerating stimuli colliding at the same time as projected for those with l/v = -20 and -80 ms, respectively. This experiment had twice as many repeats of individual stimuli as the initial one $(6, \pm 2)$. Slight differences in animal exposures to the stimuli were attributable to program errors or cessation of trials due to unresponsiveness of the subject. In total and across both experiments, 373 trials were conducted (75, \pm 4 for each of the stimuli with l/v =-20, -50 and -80 ms, as well as the associated l/v =-20 ms accelerating, and l/v = -80 ms decelerating stimuli). In total, 21 fish were used with two that did not respond to any stimuli and were excluded from the analysis.

Fish behavioural data analysis

Escape probability, latency, and C-start angular velocity were calculated based on frame-by-frame video analysis (frame rate: 250 Hz; Fig. 1B and C). Stimulus onset was determined as the first frame in which the stimulus was visible in the image. Latency was calculated as the time between stimulus onset and the first detectable head movement. Peak angular velocity of the initial part of the C-shaped body bend (Stage 1; Eaton et al., 2001) was measured in ImageJ as the change in angular direction of a line running from the fish's centre of mass to the tip of the head (see also Preuss et al., 2006; Weiss et al., 2006). In each trial with a response we measured the horizontal distance between the head of the fish and the onset position of the looming stimulus in video still images.

A bivariate fit of response times vs. distance showed no correlation ($R^2 = 0.0004$; N = 221 trials).

Statistics

All tests were two-tailed. Analyses of variance were calculated using Kruskal-Wallis non-parametric tests; the resulting significance levels are reported in the text as $p_{\rm KW}$. Significance of differences in response times or threshold angles between stimuli were calculated with the Wilcoxon rank sum test and reported as p_{WRS} . For comparisons of behavioural response probabilities, significance was calculated using Fisher's exact test and values are reported as $p_{\rm FT}$. Tests of difference from zero (Fig. 7) were calculated using the Wilcoxon sign rank test and reported as p_{WSR} . Comparison between fitted η model parameters for looms and CAVs used 10,000 bootstrapped estimates from their linear fits. The reported *P* values for these comparisons, p_{ASL}, were the 'achieved significance level' (ASL) statistic for two-sample testing of equality of means with unequal variance (Algorithm 16.2 in Efron & Tibshirani, 1993). The standard deviation is abbreviated by 'SD'. The Pearson correlation coefficient is denoted by ρ_P and the *P* value of the associated test for its difference from zero by p_P .

Results

Stimuli simulating approaching threats differ widely in their characteristics

Classically, looming stimuli (or 'looms') have been defined as two-dimensional simulations on a screen of solid objects approaching on a collision course with the animal at constant speed (Schiff et al., 1962). In a plot of distance, x(t), from the eye as a function of time, they are represented by straight lines with slopes, ν < 0, since distance decreases as the object approaches. More relevant in this case is to plot the distance to the eye normalized by the half-size of the object as a function of time from movement onset, y(t) = x(t)/l, since it is directly related to the angular size of the stimulus (Fig. 2A, green lines). The inverse of the slope in this plot, $\gamma = l/v$ – or equivalently its absolute value, l/|v| – may be used to characterize looming stimuli (in units of time; Gabbiani et al., 1999). Typical values triggering escape prior to collision in grasshoppers range from -20 to -120 ms (Fotowat & Gabbiani, 2007). In goldfish, prior experiments used values ranging from -10 to -50 ms to trigger escape (Preuss et al., 2006). The experiments described below used stimuli with $\gamma = -80, -70, -50, -30 \text{ and } -20 \text{ ms}$ for both grasshoppers and goldfish. Sensory stimulation on the animal's retina is governed by the angular size subtended by the object, which may be computed from the normalized distance by trigonometry (Fig. 1A; eqn (1), Methods). For looming stimuli, the linear decline in distance results in a non-linear, nearly exponential increase in angular size as collision time nears (Fig. 2B, green lines).

In addition to these looming stimuli, we simulated objects that either accelerate or decelerate during approach (with the acceleration or deceleration, a, constant). We call these stimuli non-zero acceleration stimuli (NZAs; see Methods for details). Two accelerating $(\gamma_c = -30 \text{ and } -20 \text{ ms})$ and two decelerating $(\gamma_c = -80 \text{ and } -70 \text{ ms})$ stimuli were used. Because at any given time before collision such a decelerating stimulus is closer than the looming stimulus with matching collision time, its angular size subtended at the eye is larger than that of the matching looming stimulus. The opposite holds for accelerating stimuli (Fig. 2B). Although NZAs have not yet been used experimentally, the normalized acceleration observed in prey capture attempts of vinegar flies by damselflies ranged from -2.14 to 0.71 s⁻² (highest acceleration and lowest deceleration, respectively; sec. 5, Gabbiani et al., 2023; von Reyn et al., 2014). Hence our ρ values span a range encompassing what has been observed in these freely behaving insects.

The final set of stimuli used for behavioural and electrophysiological experiments in grasshoppers had a constant angular velocity (ψ ; Fig. 2C, D). Hence, their angular half-size grows linearly from its initial value to reach 90° at collision time (Fig. 2D). The corresponding normalized distance reveals that they represent objects approaching rapidly initially, but then exhibiting strong time-dependent deceleration well ahead of collision time (Fig. 2C). We call such stimuli constant angular velocity stimuli (CAVs).

14697793, 2023, 19, Downloaded from https://physox.onlinelibrary.wiley.com/doi/10.1113/IP284022 by University Of Texas - Ham/Tmc, Wiley Online Library on [24.05.2024]. See the Terms and Conditions (https://onlinelibrary.wiley.com/terms-and-conditions) on Wiley Online Library for rules of use; OA articles are governed by the applicable Creative Commons Licensee and Conditions (https://onlinelibrary.wiley.com/terms-and-conditions) on Wiley Online Library for rules of use; OA articles are governed by the applicable Creative Commons Licensee and Conditions (https://onlinelibrary.wiley.com/terms-and-conditions) on Wiley Online Library for rules of use; OA articles are governed by the applicable Creative Commons Licensee and Conditions (https://onlinelibrary.wiley.com/terms-and-conditions) on Wiley Online Library for rules of use; OA articles are governed by the applicable Creative Commons Licensee and Conditions (https://onlinelibrary.wiley.com/terms-and-conditions) on Wiley Online Library for rules of use; OA articles are governed by the applicable Creative Commons Licensee and Conditions (https://onlinelibrary.wiley.com/terms-and-conditions) on Wiley Online Library for rules of use; OA articles are governed by the applicable Creative Commons Licensee and Conditions (https://onlinelibrary.wiley.com/terms-and-conditions) on Wiley Online Library for rules of use; OA articles are governed by the applicable Creative Commons Licensee and Conditions (https://onlinelibrary.wiley.com/terms-and-conditions) on the applicable Creative Commons (https://onlinelibrary.wiley.com/terms-and

Multiple models for neural responses to looming stimuli in different species

Modelling looming responses of LGMD neurons in grasshoppers and Mauthner neurons in fish produced related models that make equivalent predictions of response timing for looms but not NZAs. These models have been recently described in detail (Gabbiani et al., 2023). In grasshoppers, the LGMD/DCMD neurons are responsible for triggering jump escape behaviours to looming stimuli (Fotowat et al., 2011). The peak firing rate of these neurons comes a fixed neural delay after the looming stimulus reaches a threshold angular size, independent of the stimulus parameter γ (or equivalently, of its approach speed assuming a fixed half-size, l). A phenomenological model, called the η model, predicts this key aspect of their firing rate (Gabbiani et al., 1999;

14697793, 2023, 19, Downloaded from https://physox.onlinelibrary.wiley.com/doi/10.1113/IP284022 by University Of Texas - Ham/Imc, Wiley Online Library on [24/05/2024]. See the Terms and Conditions (https://onlinelibrary.wiley.com/terms-and-conditions) on Wiley Online Library for rules of use; OA atticles are governed by the applicable Creative Commons License

Sun & Frost, 1998). In this model, the time-dependent firing rate is (up to a scaling factor) obtained by multiplying the angular speed of the object during approach by a non-linear function of its angular size:

$$\eta(t) = \dot{\theta}(t - \delta) \exp(-\alpha \theta(t - \delta)),$$

where δ is a neural delay between stimulus and response, θ is the half-angle (Fig. 1A), and $\dot{\theta}$ is the angular speed. The parameter α determines the threshold angular size, as will become clear shortly. The η model predicts a firing rate that increases initially because $\dot{\theta}$ increases during the simulated approach. Yet, the object's angular size also increases during approach. As a result, its negative exponential rapidly becomes vanishingly small, eventually turning off the η model's response after it reaches a peak value (Fig. 2E). The timing of the firing rate peak is obtained by setting the time derivative of $\eta(t)$ to zero, yielding the condition:

$$\ddot{\theta}(t - \delta) = \alpha \dot{\theta}^2(t - \delta) \tag{2}$$

(sec. 4, Gabbiani et al., 1999; Gabbiani et al., 2023). For looming stimuli, both $\dot{\theta}$ and $\ddot{\theta}$ may be computed from the normalized distance y(t), leading to a linear relation between peak time, $t_{\rm p}$ and γ :

$$t_{\rm p} - \delta = \frac{\alpha}{2} \gamma$$
.

Because the normalized distance, $y(t)=t/\gamma$, is also a linear function of time with proportionality constant $1/\gamma$, these two γ dependences cancel out when $t=t_{\rm p}-\delta$ and the normalized distance is independent of γ , namely $y(t_{\rm p}-\delta)=\alpha/2$. Equivalently, the half-angle at $t_{\rm p}-\delta$ is given by

$$\theta\left(t_{\mathrm{p}}-\delta\right)=\tan^{-1}\left(2/\alpha\right)$$
, independent of γ .

Various aspects of this phenomenological model have been tested experimentally (Gabbiani et al., 1999), including its possible mechanisms of biophysical implementation (Gabbiani et al., 2002; Jones & Gabbiani, 2010, 2012).

For goldfish a different model describing the membrane potential during looming was proposed, called the κ model (Preuss et al., 2006). In this model the membrane potential is (up to a scaling factor) a product of the stimulus angular size by a negative exponential of angular size:

$$\kappa(t) = \theta(t) \exp(-\beta \theta(t)),$$

where we have omitted the neural delay δ for simplicity. Just as for the η model, this non-linear combination leads to an initial increase of $\kappa(t)$ followed by a peak and an eventual decrease (Fig. 2*E*). The peak condition is obtained as for the η model,

$$\theta\left(t_{\mathrm{p}}\right) = 1/\beta. \tag{3}$$

Thus, although the two models are different, they both predict a constant angular stimulus size at the peak time of their respective η and κ functions for looming stimuli (apart from a neural delay).

The η and κ models predict distinct responses to NZAs

The η and κ models make identical predictions on the timing of peak responses for looming stimuli and are thus difficult to tease apart. But could their predictions diverge for other simulated approaching stimuli such as NZAs? That this is indeed the case may be seen by examining eqns (2) and (3). The peak condition for the κ model (eqn (3)) is directly constraining the angular half-size of the stimulus. Thus, peak responses always occur at a fixed threshold angular half-size, irrespective of stimulus type. In contrast, eqn (2) for the η model requires a specific relation between angular acceleration and speed during the simulated approach. This relation will not be fulfilled at the same time for NZAs and looming stimuli since the time dependence of their angular acceleration and angular speed differ (Fig. 2F).

The peak time of the η and κ models for NZAs can be computed analytically (sec. 5, Gabbiani et al., 2023). Assuming an angular half-size threshold of 12.5° as is typical for the DCMD peak firing rate, we find that both models predict earlier peak times for decelerating stimuli and later peak times for accelerating ones than for looming stimuli with the same γ value at collision time (Fig. 2G). For the κ model this can be explained by noting that the angular size of a decelerating stimulus is always larger than that of its matching looming stimulus (with parameter γ_c ; Fig. 2B). Thus, its peak angular threshold size must occur first. Conversely, the angular size of an accelerating stimulus is always smaller than that of the matching looming stimulus and thus its peak threshold angular size must occur closer to collision time (Fig. 2H). Hence, both the η and κ models predict a distinct arrangement of peak times for NZAs and looming stimuli that has not yet been tested experimentally.

Further, and as suggested by eqns (2) and (3), the peak times in response to NZAs differ between the two models, with those of the η model occurring earlier for decelerating stimuli than those of the κ model and vice versa for accelerating stimuli. The difference between the peak times predicted by the two models was, however, small for accelerating stimuli (\sim 1 ms; see Fig. 2G, γ > -50 ms). For decelerating stimuli, it increased with stronger deceleration (compare blue and ochre lines in Fig. 2G for γ < -50 ms). Thus the η model does not predict a constant angular threshold peak for NZAs, in contrast to the κ model (Fig. 2H). Analysis of surrogate data sets generated by the η and κ models using the previously described variability of DCMD responses

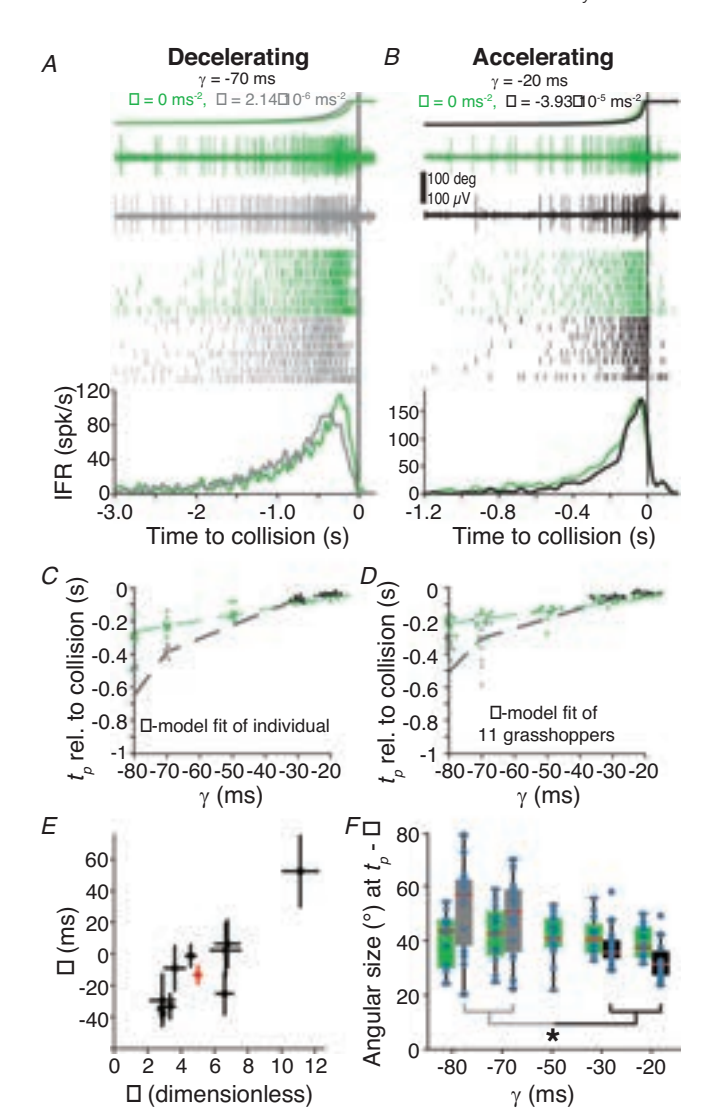
(Gabbiani et al., 1999) suggested that the two models might be distinguishable experimentally (sec. 5, Gabbiani et al., 2023).

Grasshopper neural responses to NZAs are consistent with the η model

To test whether the LGMD/DCMD neurons follow the predictions of the η or κ model, we recorded the DCMD spiking response to the looms and NZAs described above. Responses to decelerating stimuli were similar to looming responses, initially increasing and then decaying before collision time (Fig. 3A). Yet, the bulk of spikes occurred earlier than for their matched looms and so did the time of peak firing rate, as predicted by both models. The responses to accelerating stimuli also followed the general trend predicted by the models, with a tighter clustering of spikes and a peak firing rate slightly closer to collision time than for looms (Fig. 3B). For each animal, the peak times of responses to looms as a function of γ were fitted with a straight line, yielding a slope parameter, α , and a *y*-intercept, δ (Fig. 3*C*, green crosses and dashed line). The peak time responses to NZAs predicted by the η model based on these parameters yielded satisfactory fits as well (Fig. 3C, black/grey crosses and grey dashed line). A fit of mean peak time responses for each animal and each y value also yielded satisfactory fits and predicted well responses to NZAs (Fig. 3D). The range of values for the parameters α and δ obtained from these experiments agreed with those found in previous studies (Fig. 3E; e.g. Gabbiani et al., 1999). The angular threshold size computed from these fits were not significantly different from one another for looms (Fig. 3F). In contrast, NZAs yielded significantly different values for accelerating and decelerating NZAs, consistent with the η model but not with the κ model.

Grasshopper jump escape behaviour differs for NZAs and looms

We next compared the jump escape behaviour of grasshoppers to looms and NZAs. In these experiments, grasshoppers jumped in response to 58% of looms, 58% of decelerating NZAs and 50% of accelerating NZAs (Fig. 4A). No difference was detected among these three values ($p_{\rm KW}=0.61$) and the last two jump probabilities were not significantly different either ($p_{\rm FT}=0.21$). As predicted by the η and κ models, the jump times occurred earlier for decelerating, and later for accelerating NZAs than for their matched looms (Fig. 4B). Consistent with observations made on looms over the same range of γ values (Fotowat & Gabbiani, 2007; Gabbiani et al., 1999), the jump time variability was higher for decelerating than accelerating NZAs. The observed differences reached statistical significance only for the largest deceleration



14697793, 2023, 19, Downloaded from https://physoc.onlinelibrary.wiley.com/doi/10.1113/JP284022 by University Of Texas - Ham/Tmc, Wiley Online Library on [24.05.2024]. See the Terms and Condi

and-conditions) on Wiley Online Library for rules of use; OA articles are governed by the applicable Creative Commons I

Figure 3. Grasshopper neural responses to NZAs are consistent with the η model

A, top, the angles of simulated objects approaching at constant velocity (looms, green) and decreasing approach velocity (decelerating NZAs, grey). Immediately below, from top to bottom, example nerve cord recordings, spike rasters, and plot of average instantaneous firing rate (IFR) show DCMD responses to the two stimuli. The peak response time was earlier for decelerating NZAs. B, responses to stimuli with increasing approach velocity (accelerating NZAs, black) were delayed relative to constant velocity stimuli with the same γ (looms, green). Data from the same animal as shown in A. C, peak DCMD response times of each trial (crosses) and the best fit η function for the animal shown in A and B (dashed lines). D, fit of the population data; crosses are the mean response of each animal. In C and D, data points have been shifted horizontally to improve visibility. Green discs and grey triangles are mean of data points. E, the best fit α and δ parameters \pm their bootstrapped standard errors for each grasshopper (black) and the population (red). F, the threshold angular size preceding the peak DCMD response for each stimulus. Constant velocity stimulus responses had angular thresholds independent of the stimulus parameter γ ($p_{KW} = 0.96$). The response angle associated with NZAs changed with acceleration ($p_{KW} = 0.01$). (For D–F, N = 11 animals.)

14697793, 2023, 19, Downloaded from https://physoc.onlinelibrary.wiley.com/doi/10.1113/JP284022 by University Of Texas - Ham/Tmc, Wiley Online Library on [24.05.2024]. See the Terms and Conditions (https://onlinelibrary.wiley

-and-conditions) on Wiley Online Library for rules of use; OA articles are governed by the applicable Creative Commons I

and acceleration values. As reported in freely behaving flies, the probability of escape before collision was smaller for accelerating than decelerating stimuli (Fig. 4*C*; von Reyn et al. 2014). It was also larger for stimuli with lower approach velocities than for stimuli with higher approach velocities (smaller, resp. larger γ values for fixed l; Fig. 4*C*).

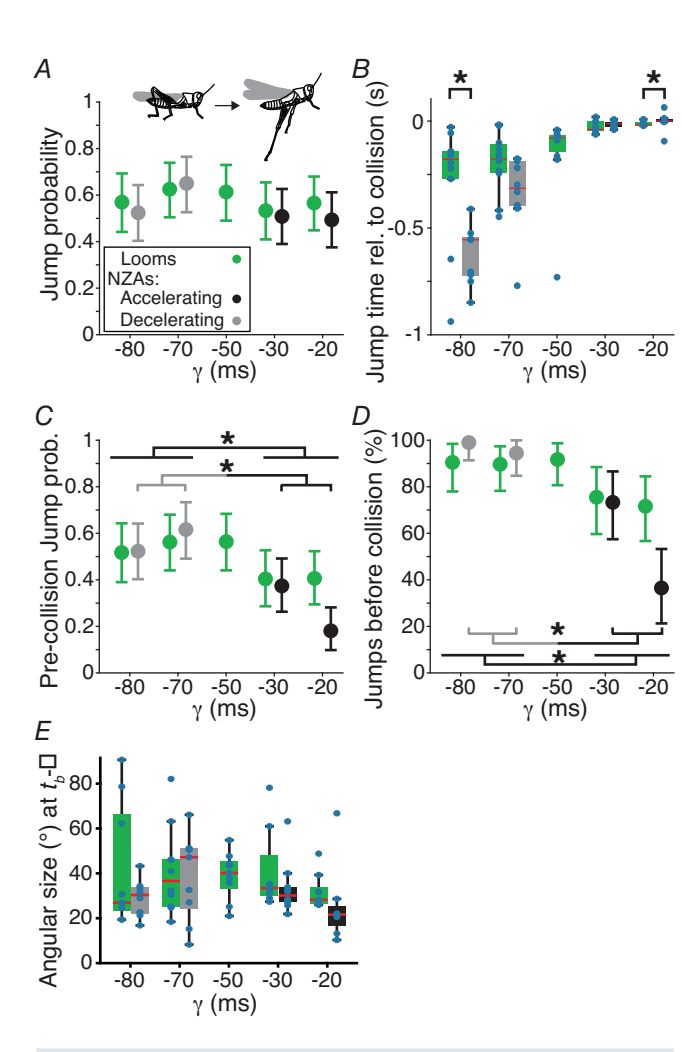


Figure 4. Grasshopper jump escape behaviour differs for NZAs and looms

A, grasshoppers jumped in response to all stimuli with similar probability ($p_{KW} = 0.61$). B, stimulus acceleration changed the response time. Acceleration produced later jumps and deceleration produced earlier jumps (* p_{WRS} < 0.05). C, the probability of producing jumps before the time of collision differs across stimuli $(p_{KW} = 0.007)$ with fewer jumps before collision for accelerating stimuli than decelerating ones (* $p_{FT} = 2.6 \times 10^{-6}$) and for faster stimuli ($\gamma > -50$ ms) *versus* slower ones ($\gamma < -50$ ms; * $p_{\text{FT}} = 1.3 \times 10^{-6}$). D, faster stimuli similarly produced a lower percentage of jumps that occurred before the time of collision; decelerating stimuli elicited higher jump percentages before collision than accelerating ones (* $p_{FT} = 1.4 \times 10^{-9}$) and percentages for $\gamma < -50$ ms were higher than for $\gamma > -50$ ms (* p_{FT} = 4.6 imes 10 $^{-10}$). E, there was no difference in response threshold angle for looms $(p_{KW} = 0.69; \delta = 57 \text{ ms}) \text{ or among NZAs } (p_{KW} = 0.18). N = 11$ animals for all plots. t_b : time of escape behaviour.

The fraction of 'successful' escape jumps, defined as those occurring before collision, was also higher for decelerating than accelerating NZAs, as well as for stimuli with lower approach velocities (smaller γ values, Fig. 4D). Fitting a straight line to the escape behaviour time relative to collision as a function of γ yielded an estimated slope, α , and a γ -intercept, δ , as for the time of peak DCMD response. The associated threshold angle at a delay δ prior to escape was more variable than that of peak DCMD firing and not significantly different across looms (Fig. 4E; compare with Fig. 3F). In contrast to the DCMD peak firing threshold angle, no significant differences were observed in escape threshold angles for NZAs (Fig. 4E). Thus, grasshopper escape behaviour follows more closely the κ than the η model.

Fish escape behaviour to NZAs is more consistent with the κ than the η model

Similar to grasshoppers, the probability of escape to looms and NZAs was comparable in goldfish with responses to 69% of looms, 72% of accelerating NZAs, and 73% of decelerating NZAs (Fig. 5A). In contrast to the predictions of the η and κ model, we observed no significant difference in escape timing when comparing accelerating or decelerating NZAs with looms (Fig. 5B). We used the same linear fitting procedure applied to grasshopper peak DCMD firing and jump escape times to estimate the threshold angle triggering escape, and the delay between this angular threshold and behaviour. No significant differences in threshold angles were found within or between looms and NZAs (Fig. 5C).

The C-start escape turns triggered by the Mauthner cell usually result in peak angular turn speeds in excess of 3000°/s (Eaton et al., 1981; Preuss et al., 2006; Weiss et al., 2006). For looms and decelerating NZAs, we found a positive correlation between escape time relative to collision and angular turn speed (Fig. 5D). A similar analysis could not be carried out for accelerating stimuli as the triggered escape behaviours clustered close to projected collision and were thus not sufficiently spread out in time to assess correlation between these two variables. Indeed, across stimuli, the fast bends occurred later than the slow bends ($p_{WRS} = 3.7 \times 10^{-7}$). Only 18% of early responses (>1.75 s before collision) were fast bends, whereas 70% of them were in the last 1.75 s before collision. The fast bend escape timing of NZAs and looms were more similar to the predictions of the η and κ models, with decelerating NZAs responses occurring earlier than those of looms (Fig. 5E). There were no differences in the threshold angles for the fast turn responses within or between looms and NZAs (Fig. 5F). This constant threshold angle independent of acceleration matches the prediction of the κ model.

Fish respond to faster stimulus expansion with more fast bends

Since most fast bend escape responses occurred closer to the time of collision, this suggested that a larger fraction of fast, Mauthner-mediated C-starts might occur for faster approaching stimuli (larger γ values). To confirm this hypothesis, we examined the probability of slow and fast bend responses for looms and NZAs. Slower expanding stimuli ($\gamma < -50$ ms) produced more slow turn responses (Fig. 6A). Similarly, decelerating stimuli produced more slow turns than did accelerating ones (Fig. 6A). Conversely, faster stimuli and accelerating ones produced a higher probability of fast turns (Fig. 6B). The majority of escape responses recorded in our experiments had peak bend velocities over 3000°/s, indicating that they are probably initiated by the Mauthner neuron. The

fraction of putative Mauthner initiated escapes increased with stimulus speed (i.e. for larger γ values; Fig. 6C). A modest positive linear trend was found between fast turn fraction and the stimulus parameter γ ($\rho_P=0.26$, $p_P=5.8\times10^{-7}$). These data suggest that faster or accelerating predator approaches are more likely to activate the Mauthner cell, in agreement with zebrafish results and similar to the increase in GF activation observed in flies for these stimuli (Bhattacharyya et al., 2017; von Reyn et al., 2014).

Within-animal comparisons of response timings further refine population results

For each grasshopper and goldfish, we examined the within-animal change in response timing between

14697793, 2023, 19, Downloaded from https://physoc.onlinelibrary.wiley.com/doi/10.1113/JP284022 by University Of Texas - Ham/Tmc, Wiley Online Library on [24.05.2024]. See the Terms and Conditions

iditions) on Wiley Online Library for rules of use; OA articles are governed by the applicable Creative Commons I

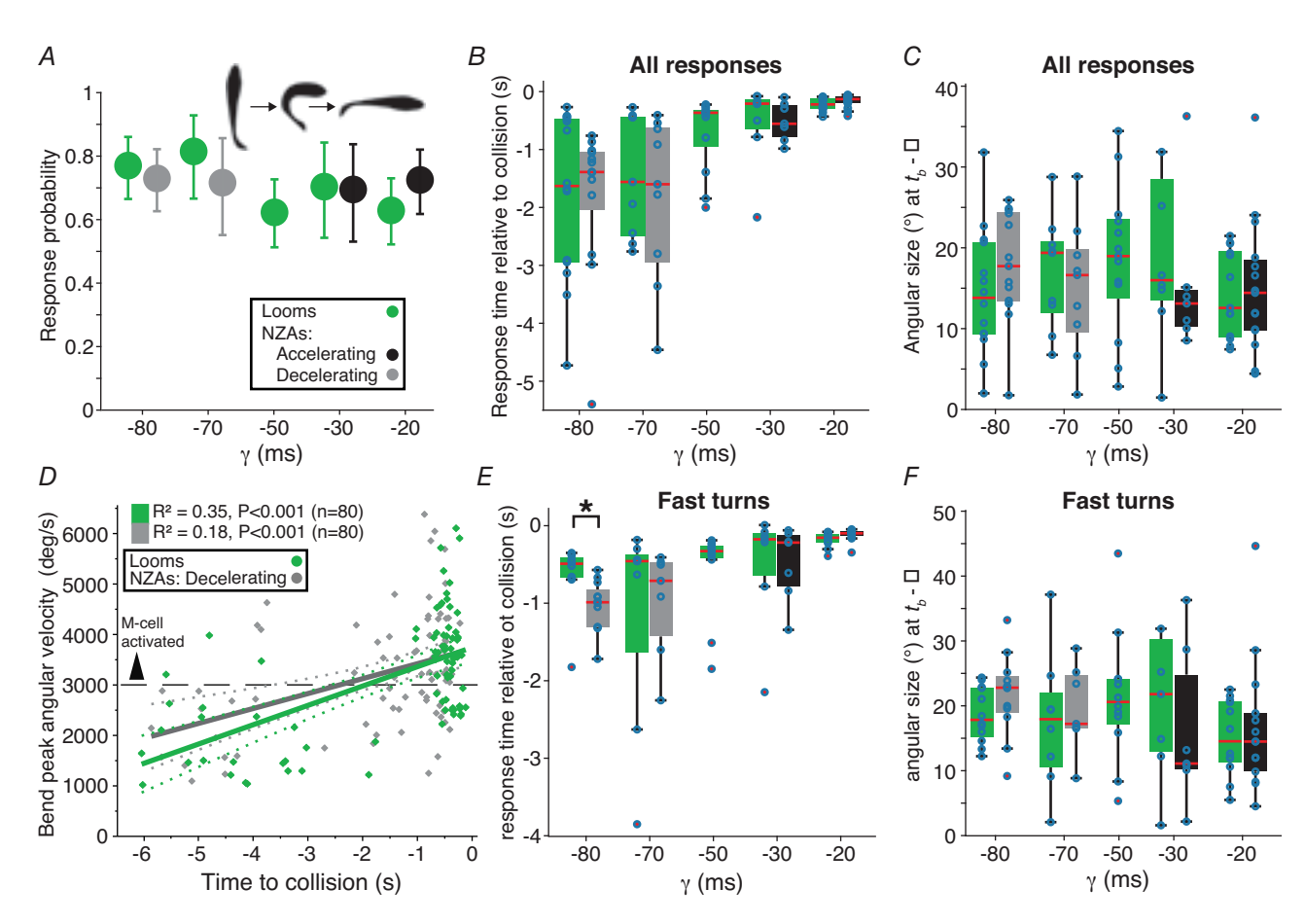


Figure 5. Fish escape behaviour to NZAs is more consistent with the κ than the η model A, C-start (inset) probability was comparable for all loom approach velocities ($\rho_{KW}=0.38$). B, response timing changed with γ for both looms and NZAs ($\rho_{KW}<0.001$), but the NZAs escape timings did not differ from their paired looms ($\rho_{WRS} \geq 0.16$). C, the response threshold angle ($\delta=25$ ms) was comparable across stimuli ($\rho_{KW}=0.67$) without significant differences between looms and NZAs with equal γ values ($\rho_{WRS} \geq 0.15$). D, the peak angular velocity of C-starts increased for responses occurring closer to collision time. Dashed horizontal line indicates C-starts with velocity over 3000°/s which typically are initiated by the Mauthner neuron (see Fig. 1 C). E, the timing of fast turns in response to NZAs differed from looms with equal γ only for the largest deceleration ($\gamma=-80$ ms; * $\rho_{WRS}=0.002$). F, the threshold angle for fast turns was not different across looms ($\rho_{KW}=0.38$) or NZAs ($\rho_{KW}=0.18$). N=19 animals for all plots.

14697793, 2023, 19, Downloaded from https://physoc.onlinelibrary.wiley.com/doi/10.1113/JP284022 by University Of Texas - Ham/Tmc, Wiley Online Library on [24.05.2024]. See the Terms and Condi

iditions) on Wiley Online Library for rules of use; OA articles are governed by the applicable Creative Commons License

looms and NZAs of equal γ . For neural responses in grasshoppers, acceleration delayed peak firing and deceleration produced earlier peaks, changes consistent with both the η and κ models (Fig. 7A, left). The influence of acceleration on the timing of grasshopper behaviour was similar to that of the neural response (Fig. 7A, centre). The goldfish behaviour showed no consistent change in

response timing with acceleration, inconsistent with either model prediction (Fig. 7A, right).

The threshold angle of the grasshopper neural response was changed by acceleration (Fig. 7*B*, left). This change is inconsistent with the κ model, but, unexpectedly, the direction of the change was not that predicted by the η model (cf. Fig. 2*H*). For grasshopper behaviour,

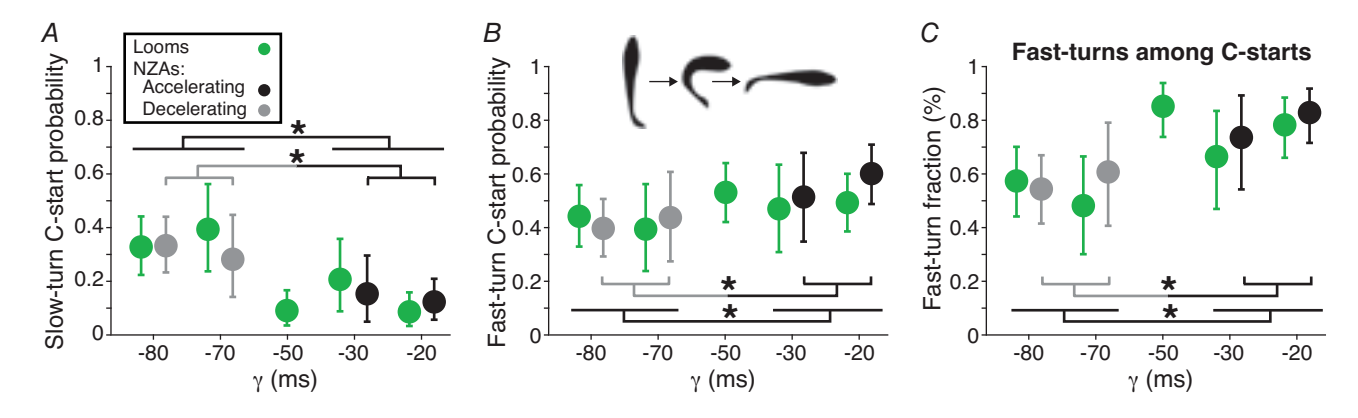


Figure 6. Fish respond to faster stimulus expansion with more fast bends A, the probability of slow-turn C-starts was higher for slower simulated approaches; the slow-turn probability for $\gamma < -50$ ms was higher than for $\gamma > -50$ ms (* $p_{\text{FT}} = 1.1 \times 10^{-5}$) and the slow-turn probability for accelerating stimuli was lower than for decelerating ones (* $p_{\text{FT}} = 0.002$). B, conversely, the probability of fast-turn C-starts was higher for faster simulated approaches; it was higher for accelerating than decelerating stimuli (* $p_{\text{FT}} = 0.014$) and it was also higher for $\gamma > -50$ ms than for $\gamma < -50$ ms (* $p_{\text{FT}} = 0.005$). C, the fraction of fast-turns among all C-start responses also increased as the simulated approach velocity increased; it was higher for accelerating than

decelerating stimuli (* p_{FT} = 0.0009) and it was higher for $\gamma > -50$ ms than for $\gamma < -50$ ms (* p_{FT} = 2.0 \times 10⁻⁶).

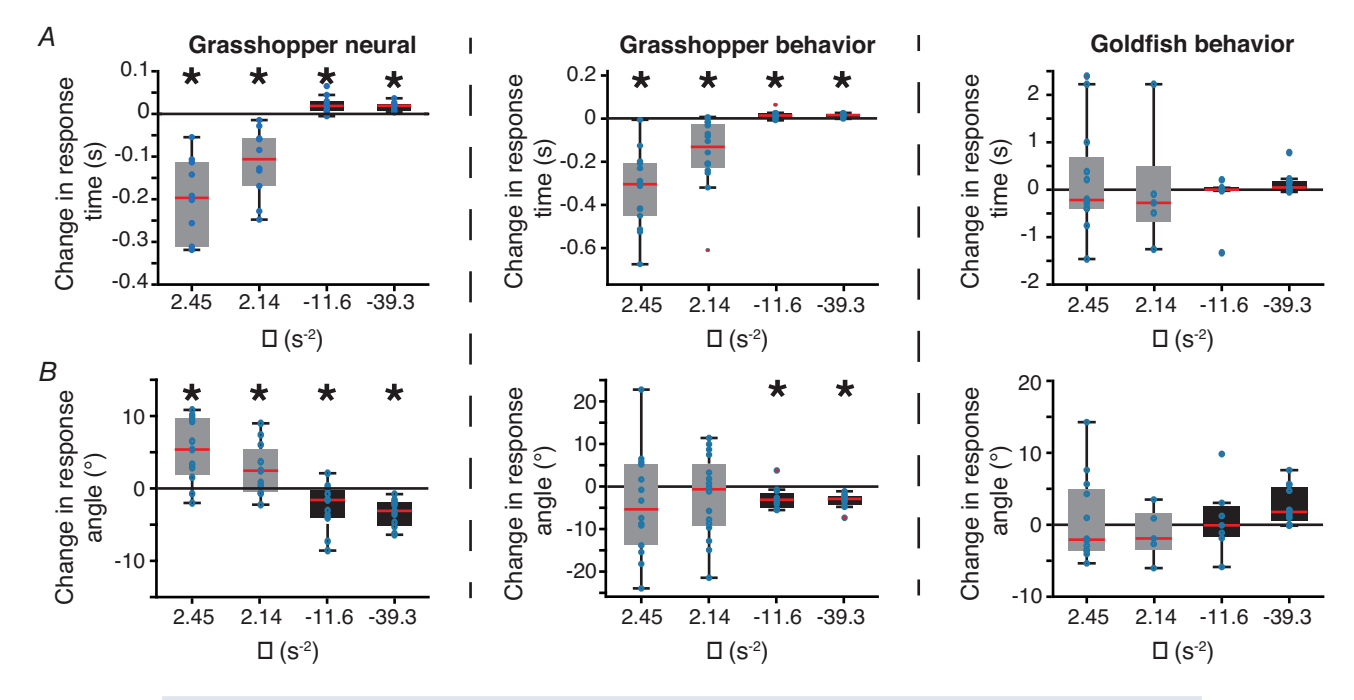


Figure 7. Within-animal comparisons of response timings further refine population results A, within-animal comparisons showed that grasshoppers responded later to accelerating stimuli (black boxes) and earlier to decelerating stimuli (grey boxes) whereas no timing difference was found in fish. B, within animal comparisons of the threshold angle of grasshopper neural responses showed an increase with deceleration relative to looms. In contrast, the threshold angle at behavioral onset was not affected by acceleration in either species. $*p_{WSR} < 0.05$.

the median threshold angle was smaller for the two accelerating stimuli, matching the neural timing (Fig. 7*B*, centre). The goldfish response threshold angle was unchanged by stimulus acceleration, consistent with the κ but not with the η model prediction (Fig. 7*B*, right).

CAVs elicit different timings for neural and behavioural responses in grasshoppers

The grasshopper neural responses to NZAs showed changes in timing that were acceleration dependent, and more consistent with the η than the κ model. The timing of the grasshopper behavioral response was inconclusive for distinguishing the models. We thus used constant angular velocity stimuli (CAVs), as the η and κ models predict large timing differences for them (Fig. 2*H*). Specifically, the η model predicts a peak response to CAVs a fixed delay (δ) after the stimulus begins expanding, while the κ model predicts a peak response at a delay δ after a threshold angular size, and hence a delay from stimulation onset that decreases with increasing angular velocity (sec. 6, Gabbiani et al., 2023).

Looms produced the characteristic ramp up and decrease in firing rate as the stimulus expanded (Fig. 8A). In contrast, CAVs produced firing patterns that increased quickly to a peak and then decayed more slowly (Fig. 8B). The time of peak responses to CAVs was independent of the expansion speed unlike for looms (Fig. 8C). The threshold angle was fixed for looms but changed with the angular speed of CAVs (Fig. 8D). The timing and angular thresholds extracted from these data confirm that the η model best describes the grasshopper neural response.

The same stimuli were presented to freely moving grasshoppers which jumped equally to both looms and CAVs (Fig. 8*E*). The timing of the behavioural response matched that of the neural response for looms but not for CAVs (Fig. 8*F*). The escape jumps from CAVs did not come a fixed delay after the start of expansion, but instead after the same threshold angle as for looms (Fig. 8*G*). Estimating best η fits for grasshopper escape times for looms and CAVs yielded no difference in δ ($p_{\rm ASL} = 0.41$) or threshold angle ($p_{\rm ASL} = 0.30$). These data show that while the grasshopper's neural response timing to CAVs is better predicted by the η model, the behavioural timing is better described by the κ model.

Previous work on the sensory-motor transformations leading to escape jumps for looms in grasshoppers has suggested that the decrease in firing following the DCMD peak rate is key in triggering the jump, presumably because it results in decreased flexor excitation (Fotowat & Gabbiani, 2011). We therefore examined averaged neural response profiles to see how they related to the timing of jump escape. As expected, jumps in response to looms occurred on average during the decaying phase of the

DCMD response (Fig. 8Ha). Although neural responses to CAVs peaked at the same time, their decrease from peak slowed with decreasing stimulus angular velocity (Fig. 8Hb). The variable rate of decay resulted in an average behavioural response timing occurring at a similar fractional decay from the peak firing rate (\sim 20% on average; Fig. 8Hb).

Discussion

We used two new classes of laboratory stimuli to study the responses of collision-detecting neurons and escape behaviours in grasshoppers and goldfish. For both species, the timing of escape behaviour across stimuli was consistent with responding a fixed delay after the stimulus surpasses an angular threshold size as predicted by the κ model. For grasshoppers the timing of the neural response to all three stimulus types changed with acceleration, consistent with the η model.

The first stimulus class, NZAs, is built on classical looming stimuli by adding constant acceleration or deceleration to interpolate between different initial and final γ values. NZAs were inspired by the observation that predator approach trajectories accelerating towards their prey lead to less successful escape behaviours of freely behaving vinegar flies, and vice versa for deceleration (von Reyn et al., 2014). Our experiments establish a similar result in a controlled setting for grasshoppers, as accelerating stimuli produce more escapes after the projected collision time (Fig. 4). In contrast, the escape behaviour of goldfish shows a considerably reduced sensitivity to acceleration and deceleration, and all escapes occurred before projected collision.

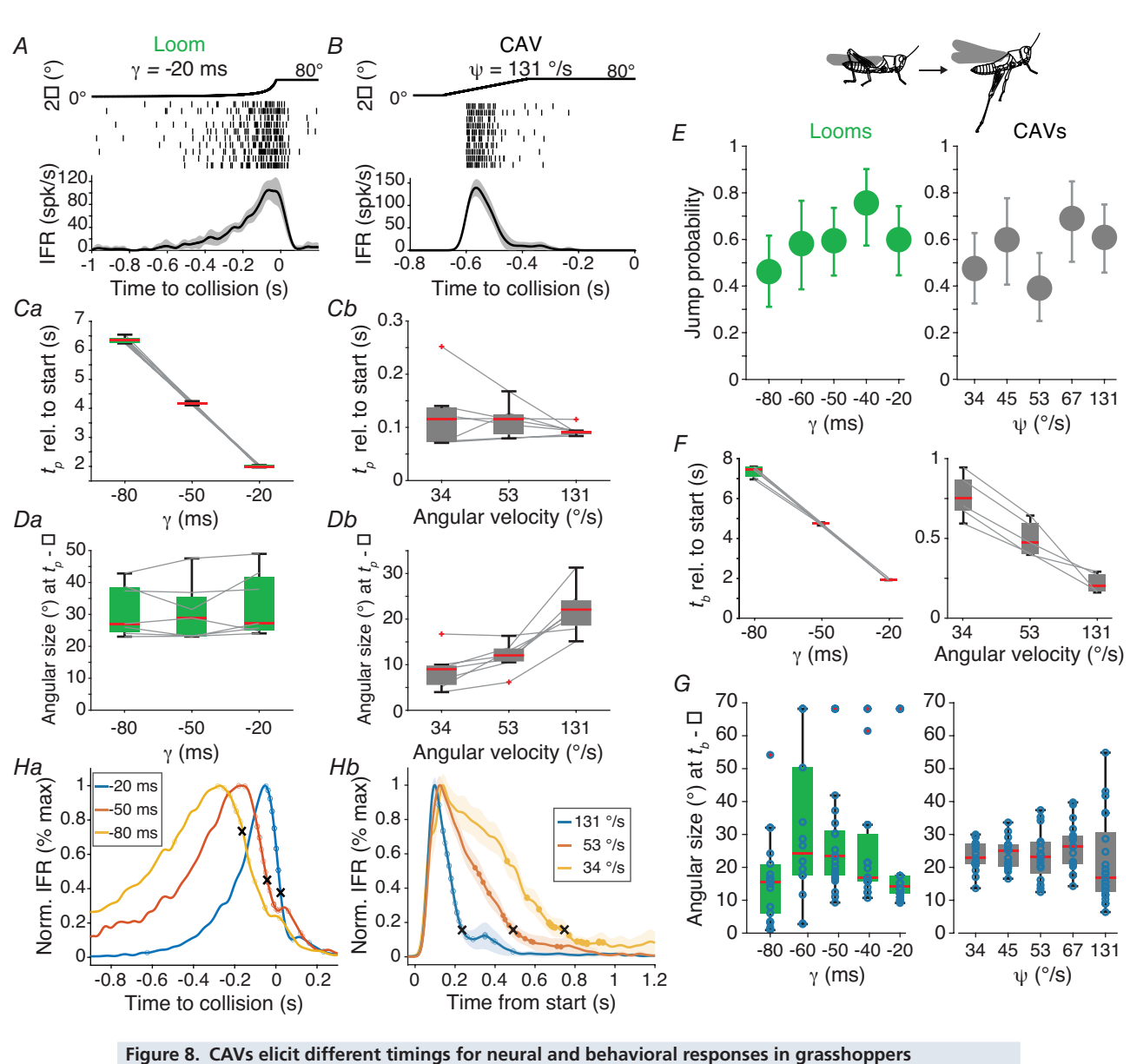
14697793, 2023, 19, Downloaded from https://physox.onlinelibrary.wiley.com/doi/10.1113/IP284022 by University Of Texas - Ham/Imc, Wiley Online Library on [24.05/2024]. See the Terms and Conditions (https://onlinelibrary.wiley.com/terms-and-conditions) on Wiley Online Library for rules of use; OA articles are governed by the applicable Creative Commons License

The second stimulus class, CAVs, borrows from stimuli used to elicit escape behaviours in rodents. Those stimuli expand with constant angular velocity but typically span a small angular range (e.g. 2-20° at the animal's retina) and are usually presented in short succession 5-10 times to elicit rodent escape behaviour (Salay et al., 2018; Wei et al., 2015; Yilmaz & Meister, 2013). Here, CAVs were presented only once and expanded to cover a large fraction of the visual field like classical looming stimuli (> 80°). In grasshoppers, the use of CAVs confirmed the dichotomy between the LGMD/DCMD neural responses and behavioural escape jumps, with the former better described by the η model and the latter by the κ model. The average behavioral response timing occurred at a similar fractional decay from the peak firing rate $(\sim 20\%)$. This is consistent with previous hypotheses for the motor coordination of the jump suggesting that take-off occurs after the cessation of DCMD firing and the relaxation of the flexor muscle (Fotowat et al., 2011). Electrophysiological recordings of DCMD activity during

14697793, 2023, 19, Downloaded from https://physoc.onlinelibrary.wiley.com/doi/10.1113/JP284022 by University Of Texas - Ham/Tmc, Wiley Online Library on [24.05/2024]. See the Terms and Conditions

onlinelibrary.wiley

onditions) on Wiley Online Library for rules of use; OA articles are governed by the applicable Creative Commons I



A, representative neural responses in a grasshopper to a looming stimulus that simulates an object with constant approach velocity. Top, time course of stimulus expansion. Middle, spike rasters of DCMD activity, each line is the response to a separate trial. Bottom, instantaneous firing rates (IFR) of the DCMD response presented as mean \pm SD. B, responses of the same animal to stimuli expanding with constant angular velocities (CAVs). Data presented as in A. C, the time from the start of expansion to the peak response differs for looming stimuli of different expansion rates (Ca, $p_{KW} = 1.3 \times 10^{-4}$, N = 7), but constant angular velocity expansion produces peak response delays unchanged by expansion rate (Cb, $p_{KW} = 0.61$, N = 7). D, looming stimuli produced a peak response at a fixed angular size (modulo a time delay, δ ; Da, $p_{KW} = 0.71$, N = 7). However, the threshold angular size in response to CAVs depends on angular velocity (Db, $p_{KW} = 0.001$, N = 7). E, grasshoppers jumped in response to both CAVs and looms with equal probability. F, the jump time from the start of expansion was not constant for looms ($p_{KW} = 7.5 \times 10^{-5}$, N = 6) or CAVs ($p_{KW} = 3.5 \times 10^{-4}$, N = 6). G, the stimulus threshold size of the jump was consistent across both CAVs and looms; $\delta = 76$ ms. H, jumps occurred after the neural responses started to decay, as may be seen by comparing the average normalized IFRs in response to looms (a) and CAVs (b) with the jump times. The mean (SD) of individual peak firing rates for looms were 136.9 (27.7), 105.0 (21.2), and 91.7 (26.0) spikes/s for $\gamma = -20$, -50 and -80 ms, respectively (N = 6). The peak rates for CAVs were 168.4 (25.0), 114.3 (10.7), and 91.8 (10.1) spikes/s for $\psi=131$, 53 and 34°/s, respectively (N = 6). Individual trial and average

jump times are marked with circles and x, respectively.

behavioural response to CAVs in freely-moving animals would confirm this.

The timing of the neural responses to CAVs was a fixed delay, δ , after stimulus start as predicted by the η model, but the δ was \sim 100 ms, unlike that of looms which is \sim 25 ms (Fig. 8Cb). The neural delay between stimuli and the resulting LGMD activation is stimulus dependent, with larger and faster stimuli producing shorter delays (Jones & Gabbiani, 2010; authors' unpublished data). For looms and NZAs where the peak response occurs near the time of collision, this peak occurs when the stimulus is large and has a high angular velocity, producing short delays of \sim 25 ms. For small stimuli the delay to LGMD activation can be > 100 ms due to slower activation of the presynaptic network (Jones & Gabbiani, 2010). This is the most likely reason for the increased delay of the peak responses to CAVs compared to those of looms and NZAs. Both the decelerating NZAs and the non-constant decelerating CAVs produced earlier neural responses relative to projected collision, consistent with the η model predictions.

In grasshoppers and goldfish, two different models, η and κ respectively, have been proposed to describe the responses of the LGMD/DCMD neurons and the Mauthner cell to looming stimuli (Gabbiani et al., 1999; Preuss et al., 2006). These models are difficult to distinguish, though, because they both predict that the time of peak neuronal responses should occur apart from a time delay, δ , at a constant angular threshold size in response to looms, independent of their parameter γ . One difference between the models is that only the η model predicts a constant LGMD/DCMD number of spikes, independent of γ . In contrast, only the κ model predicts a constant peak M-cell membrane potential (sec. 5, Gabbiani et al., 2023; Preuss et al., 2006). Both predictions are in reasonable agreement with experimental observations but represent weak constraints distinguishing the models since they could be implemented in either model through a rescaling of the output by addition of a static non-linearity (sec. 5, Gabbiani et al., 2023). In contrast, the η and κ models predict different peak response times for NZAs and CAVs, thus opening the possibility of distinguishing the two models through their main predictions: the timing of peak response and the angular threshold size at peak time. Besides distinguishing the two models, NZAs allowed us to investigate the influence of stimulus acceleration on the responses of the looming sensitive LGMD/DCMD neurons in grasshoppers, as well as behavioural escape responses in grasshoppers and goldfish.

Interestingly, a different phenomenological model for the membrane potential of the *Drosophila* giant fibre (GF) in response to looming stimuli has been developed (Ache et al., 2019; von Reyn et al., 2017). By firing a single spike, this neuron, similar to the Mauthner cell, triggers a fast, short latency jump and subsequent flight escape thought to be of last resort (Card & Dickinson, 2008; Fotowat et al., 2009; von Reyn et al., 2014). In contrast to the η and κ models that multiply angular size or speed with a negative exponential of size, the GF model sums four non-linear terms representing the inputs to the GF of four classes of neurons, two excitatory and two inhibitory. Just as the η and κ models, the GF model peak membrane potential output during looming is tuned to a fixed angular size irrespective of γ (Ache et al., 2019). But for NZAs and CAVs it behaves more like the κ model rather than the η model (Figs 5 and 6, Gabbiani et al., 2023).

In grasshoppers, the neural responses of the LGMD/DCMD neurons agreed with several predictions of the η model. Specifically, peak responses to accelerating NZAs occurred later than for equivalent constant speed stimuli while peak responses to decelerating NZAs occurred earlier. Further, the angular threshold size at the peak response time was not constant for accelerating and decelerating stimuli. Yet, the predicted change in angular threshold size at the time of peak firing rate when switching from looms to NZAs was not that observed experimentally. Further, grasshopper escape behaviour to NZAs was better described by the κ model, suggesting an additional transform between the descending sensory neural activity and the motor output triggering escape jumps. In grasshoppers, we further tested neural and behavioural responses to CAVs, confirming the results obtained with NZAs that the threshold angle associated with the neural response changes with acceleration but that the behavioural response is associated with a fixed threshold angular size.

14697793, 2023, 19, Downloaded from https://physox.onlinelibrary.wiley.com/doi/10.1113/IP284022 by University Of Texas - Ham/Imc, Wiley Online Library on [24.05/2024]. See the Terms and Conditions (https://onlinelibrary.wiley.com/terms-and-conditions) on Wiley Online Library for rules of use; OA articles are governed by the applicable Creative Commons License

In goldfish, escape response times to NZAs were more variable than in grasshoppers. This may be expected since multiple pathways drive goldfish escape behaviour, in contrast to grasshoppers (Domenici & Hale, 2019; Fotowat et al., 2011). The angular threshold size preceding the escape behaviour remained relatively constant, irrespective of the accelerating or decelerating profile of the NZAs. This experimental result was consistent with the predictions of the κ model. However, the timing of escape responses showed little sensitivity to acceleration or deceleration, in contrast to κ model predictions. Yet, an increased sensitivity to NZAs could be detected for behavioural reaction times when restricting the analysis to fast bends, probably initiated by the Mauthner cell in response to faster approaches.

Thus, in both species the timing of behavioural responses was more variable and less well predicted by the η and κ models, respectively, than those of the LGMD/DCMD neurons and the Mauthner cell, as proxied by fast bends. Part of the increased variability in response timing is due to experimental variability in the exact positioning of the freely moving animals, changing the stimulus angular expansion slightly between

14697793, 2023, 19, Downloaded from https://physox.onlinelibrary.wiley.com/doi/10.1113/IP284022 by University Of Texas - Ham/Imc, Wiley Online Library on [24.05/2024]. See the Terms and Conditions (https://onlinelibrary.wiley.com/terms-and-conditions) on Wiley Online Library for rules of use; OA articles are governed by the applicable Creative Commons License

trials. Additionally there is variability in the behavioural response threshold angle, escape trajectory and escape strategy that might prevent predators from anticipating their prey's escape responses (Bateman & Fleming, 2014; Domenici et al., 2011).

Evaluating different looming detection computations raises the question of what predator detection implementations would be most effective for survival. The current lack of data on predator approach trajectories means this question cannot yet be answered precisely, but some general points can be inferred. All animals need to detect collision early enough to account both for the time required to execute the escape and the delays of neural processing. Many prey animals, including grasshoppers, are most visible to predators when fleeing and at least one bird species tries to visually evoke escapes to improve predation (Jabłoński & Strausfeld, 2001). So, prey may want to delay escape until it is necessary.

Using a constant threshold angular size to trigger escape is advantageous if the threshold angle is small enough to give time to escape and large enough to avoid most false alarms. The shift in escape timing predicted by a strict implementation of the η model may be maladaptive, in that it would cause escapes at smaller angles for decelerating approaches that require less time to flee from, and at larger angles for accelerating approaches that provide less time to escape (Fig. 2H). The more effective escape strategy would be to adopt a smaller threshold angle for accelerating stimuli, which is not accomplished by a strict implementation of either η , κ , or GF models. Grasshoppers, unexpectedly, exhibited such a decrease in threshold angular size for accelerating stimuli (Fig. 7B), suggesting there may be additional visual processing to escape accelerating predators more effectively. Despite this, though, most responses to stimuli with high acceleration occurred after the projected collision time (Fig. 4D). The speed of the Mauthner cell triggered escape response in goldfish might make such a shift in threshold angle for accelerating stimuli unnecessary as all recorded responses were before projected collision.

In summary, responses to accelerating stimuli support the η and κ models for the LGMD/DCMD neurons and the Mauthner cell, respectively, while also showing their limitations. The behavioural response of grasshoppers was better described by the κ model, though, revealing that sensory information is transformed as it interfaces with the motor system driving escape jumps. As a result, collision avoidance in grasshopper and goldfish converge towards a common escape strategy relying on angular threshold size irrespective of stimulus properties, as reflected in the κ model. The same stimuli could help disambiguate competing models of looming responses in other species and offer further insights in the neural computations underlying escape behaviours. As more is learned about the approach trajectories of predators, understanding the underlying computations serving collision-avoidance will also provide insight into the neural adaptations resulting from predator-prey interactions.

References

- Ache, J. M., Polsky, J., Alghailani, S., Parekh, R., Breads, P.,
 Peek, M. Y., Bock, D. D., von Reyn, C. R., & Card, G. M.
 (2019). Neural Basis for looming size and velocity encoding in the drosophila giant fiber escape pathway. *Current Biology*, 29(6), 1073–1081.e4.
- Bateman, P. W., & Fleming, P. A. (2014). Switching to Plan B: Changes in the escape tactics of two grasshopper species (Acrididae: Orthoptera) in response to repeated predatory approaches. *Behavioral Ecology and Sociobiology*, **68**(3), 457–465.
- Bennett, C., Gale, S. D., Garrett, M. E., Newton, M. L., Callaway, E. M., Murphy, G. J., & Olsen, S. R. (2019). Higher-order thalamic circuits channel parallel streams of visual information in mice. *Neuron*, **102**(2), 477–492.e5.
- Bhattacharyya, K., McLean, D. L., & MacIver, M. A. (2017). Visual threat assessment and reticulospinal encoding of calibrated responses in larval zebrafish. *Current Biology*, **27**(18), 2751–2762.e6.
- Branco, T., & Redgrave, P. (2020). The neural basis of escape behavior in vertebrates. *Annual Review of Neuroscience*, **43**(1), 417–439.
- Card, G., & Dickinson, M. (2008). Performance trade-offs in the flight initiation of Drosophila. *Journal of Experimental Biology*, **211**(3), 341–353.
- de Vries, S. E. J., & Clandinin, T. R. (2012). Loom-sensitive neurons link computation to action in the *Drosophila* visual system. *Current Biology*, **22**(5), 353–362.
- Dewell, R. B., & Gabbiani, F. (2018). Biophysics of object segmentation in a collision-detecting neuron. *Elife*, 7, e34238
- Domenici, P., Blagburn, J. M., & Bacon, J. P. (2011). Animal escapology II: Escape trajectory case studies. *Journal of Experimental Biology*, **214**(15), 2474–2494.
- Domenici, P., & Hale, M. E. (2019). Escape responses of fish: A review of the diversity in motor control, kinematics and behaviour. *Journal of Experimental Biology*, **222**(18), jeb166009.
- Dunn, T. W., Gebhardt, C., Naumann, E. A., Riegler, C., Ahrens, M. B., Engert, F., & Del Bene, F. (2016). Neural circuits underlying visually evoked escapes in larval zebrafish. *Neuron*, **89**(3), 613–628.
- Eaton, R. C., Lavender, W. A., & Wieland, C. M. (1981). Identification of Mauthner-initiated response patterns in goldfish: Evidence from simultaneous cinematography and electrophysiology. *Journal of Comprehensive Physiology*, **144**(4), 521–531.
- Eaton, R. C., Lee, R. K. K., & Foreman, M. B. (2001). The Mauthner cell and other identified neurons of the brainstem escape network of fish. *Progress in Neurobiology*, **63**(4), 467–485.
- Efron, B., & Tibshirani, R. J. (1993). *An Introduction to the Bootstrap*. Chapman & Hall, New York. Available at: https://doi.org/10.1007/978-1-4899-4541-9

- Fotowat, H., Fayyazuddin, A., Bellen, H. J., & Gabbiani, F. (2009). A novel neuronal pathway for visually guided escape in Drosophila melanogaster. *Journal of Neurophysiology*, **102**(2), 875–885.
- Fotowat, H., & Gabbiani, F. (2007). Relationship between the phases of sensory and motor activity during a looming-evoked multistage escape behavior. *Journal of Neuroscience*, **27**(37), 10047–10059.
- Fotowat, H., & Gabbiani, F. (2011). Collision detection as a model for sensory-motor integration. *Annual Review of Neuroscience*, **34**(1), 1–19.
- Fotowat, H., Harrison, R. R., & Gabbiani, F. (2011). Multiplexing of motor information in the discharge of a collision detecting neuron during escape behaviors. *Neuron*, **69**(1), 147–158.
- Gabbiani, F., Krapp, H. G., Koch, C., & Laurent, G. (2002). Multiplicative computation in a visual neuron sensitive to looming. *Nature*, **420**(6913), 320–324.
- Gabbiani, F., Krapp, H. G., & Laurent, G. (1999). Computation of object approach by a wide-field, motion-sensitive neuron. *The Journal of Neuroscience*, **19**(3), 1122–1141.
- Gabbiani, F., Mo, C., & Laurent, G. (2001). Invariance of angular threshold computation in a wide-field looming-sensitive neuron. *Journal of Neuroscience*, 21(1), 314.
- Gabbiani, F., Preuss, T., & Dewell, R. B. (2023). Approaching object acceleration differentially affects the predictions of neuronal collision avoidance models. *Biological Cybernetics*, **117**(1–2), 129–142.
- Hatsopoulos, N., Gabbiani, F., & Laurent, G. (1995). Elementary computation of object approach by a wide-field visual neuron. *Science*, **270**(5238), 1000–1003.
- Hemmi, J. M., & Tomsic, D. (2012). The neuroethology of escape in crabs: From sensory ecology to neurons and back. *Current Opinion in Neurobiology*, **22**(2), 194–200.
- Jabłoński, P. G., & Strausfeld, N. J. (2001). Exploitation of an ancient escape circuit by an avian predator: Relationships between taxon-specific prey escape circuits and the sensitivity to visual cues from the predator. *Brain Behavior* and Evolution 58(4), 218–240.
- Jones, P. W., & Gabbiani, F. (2010). Synchronized neural input shapes stimulus selectivity in a collision-detecting neuron. *Current Biology*, 20(22), 2052–2057.
- Jones, P. W., & Gabbiani, F. (2012). Logarithmic compression of sensory signals within the dendritic tree of a collision-sensitive neuron. *Journal of Neuroscience*, **32**(14), 4923–4934.
- Liu, Y.-J., Wang, Q., & Li, B. (2011). Neuronal responses to looming objects in the superior colliculus of the cat. *Brain, Behavior and Evolution*, 77(3), 193–205.
- Nakagawa, H., & Hongjian, K. (2010). Collision-sensitive neurons in the optic tectum of the Bullfrog, Rana catesbeiana. *Journal of Neurophysiology*, **104**(5), 2487–2499.
- Oliva, D., & Tomsic, D. (2014). Computation of object approach by a system of visual motion-sensitive neurons in the crab Neohelice. *Journal of Neurophysiology*, **112**(6), 1477–1490.
- O'Shea, M., Rowell, C. H. F., & Williams, J. L. D. (1974). The anatomy of a locust visual interneurone; the descending contralateral movement detector. *Journal of Experimental Biology*, **60**(1), 1–12.

- O'Shea, M., & Williams, J. L. D. (1974). The anatomy and output connection of a locust visual interneurone; the lobular giant movement detector (LGMD) neurone. *Journal of Comparative Physiology A: Neuroethology, Sensory, Neural, and Behavioral Physiology*, **91**(3), 257–266.
- Preuss, T., Osei-Bonsu, P. E., Weiss, S. A., Wang, C., & Faber, D. S. (2006). Neural representation of object approach in a decision-making motor circuit. *Journal of Neuroscience*, **26**(13), 3454–3464.
- von Reyn, C. R., Breads, P., Peek, M. Y., Zheng, G. Z., Williamson, W. R., Yee, A. L., Leonardo, A., & Card, G. M. (2014). A spike-timing mechanism for action selection. *Nature Neuroscience*, **17**(7), 962–970.
- von Reyn, C. R., Nern, A., Williamson, W. R., Breads, P., Wu, M., Namiki, S., & Card, G. M. (2017). Feature integration drives probabilistic behavior in the drosophila escape response. *Neuron*, **94**(6), 1190–1204.e6.e6.

14697793, 2023, 19, Downloaded from https://physoc.onlinelibrary.wiley.com/doi/10.1113/JP284022 by University Of Texas - Ham/Tmc, Wiley Online Library on [24.05.2024]. See the Terms and Conditions (https://onlinelibrary.wiley

com/terms-and-conditions) on Wiley Online Library for rules of use; OA articles are governed by the applicable Creative Commons License

- Salay, L. D., Ishiko, N., & Huberman, A. D. (2018). A midline thalamic circuit determines reactions to visual threat. *Nature*, 557(7704), 183–189.
- Schiff, W., Caviness, J. A., & Gibson, J. J. (1962). Persistent fear responses in rhesus monkeys to the optical stimulus of "looming". *Science*, **136**(3520), 982–983.
- Sun, H., & Frost, B. J. (1998). Computation of different optical variables of looming objects in pigeon nucleus rotundus neurons. *Nature Neuroscience*, **1**(4), 296–303.
- Temizer, I., Donovan, J. C., Baier, H., & Semmelhack, J. L. (2015). A visual pathway for looming-evoked escape in larval zebrafish. *Current Biology*, **25**(14), 1823–1834.
- Vijayan, S., Mitchell, W. A., Rosenzweig, M. L., Kotler, B. P., Balaban-Feld, J., Tovelem, L. T., & Abramsky, Z. (2018). Influence of prey-food abundance on predator–prey foraging games: A test with little egrets and goldfish. *Evolutionary Ecology Research*, **19**, 455–468.
- Wei, P., Liu, N., Zhang, Z., Liu, X., Tang, Y., He, X., Wu, B., Zhou, Z., Liu, Y., Li, J., Zhang, Y., Zhou, X., Xu, L., Chen, L., Bi, G., Hu, X., Xu, F., & Wang, L. (2015). Processing of visually evoked innate fear by a non-canonical thalamic pathway. *Nature Communications*, **6**(1), 6756.
- Weiss, S. A., Zottoli, S. J., Do, S. C., Faber, D. S., & Preuss, T. (2006). Correlation of C-start behaviors with neural activity recorded from the hindbrain in free-swimming goldfish (Carassius auratus). *Journal of Experimental Biology*, **209**(23), 4788–4801.
- Wu, L.-Q., Niu, Y.-Q., Yang, J., & Wang, S.-R. (2005). Tectal neurons signal impending collision of looming objects in the pigeon. *European Journal of Neuroscience*, **22**(9), 2325–2331.
- Yilmaz, M., & Meister, M. (2013). Rapid innate defensive responses of mice to looming visual stimuli. *Current Biology*, **23**(20), 2011–2015.

Additional information

Data availability statement

All data presented in the manuscript and the Matlab code to generate the figures is available on Mendeley Data (repository DOI: 10.17632/89s2ss2wzk.1).

Competing interests

The authors have no conflicts of interest to report.

Author contributions

F.G., R.B.D., and T.P. designed the work. R.B.D., T.C.-M., M.R.E., A.F.M., and B.H. carried out the experiments and analyzed the data. R.B.D., F.G., and T.P. wrote the manuscript, with additional input from T.C.-M. and M.R.E. All authors approved the final version of the manuscript. All persons designated as authors qualify for authorship, and all those who qualify for authorship are listed.

Funding

Supported by NSF grant DBI-2021795 and NIH grant R01NS130917 to FG.

Acknowledgements

Thanks to Ms Gona Kordestani for technical help with grasshopper experiments. Thanks to the BCM Bioengineering Core for aid in experimental design (supported through an NEI Core Grant for Vision Research, EY-002520-37).

Keywords

collision-avoidance, DCMD, giant fibre, LGMD, looming, Mauthner cell, neuron models

Supporting information

Additional supporting information can be found online in the Supporting Information section at the end of the HTML view of the article. Supporting information files available:

Statistical Summary Document Peer Review History